Supporting Information

Electron repulsion tuned electronic structure of TiO_2 by fluorination for efficient and selective photocatalytic ammonia generation

*Huiling Zhu [a], Xiangran Xu [a], Yongchao Wang [a], Jian Ding [a], Xinru Yu [a], Xiaoyi Liu [a], Zhaowu Zeng [a], Huan Wang [a], Zhen Li [a], Yang Wang [a]**

a Faculty of Materials Science and Chemistry, China University of Geosciences, Wuhan, 430074 PR. China. (wyisian@cug.edu.cn)

Characterizations

X-ray powder diffraction (XRD, Bruker D8 Advance) and Raman (Bruker R2000-L) were employed to analyze the phase and defect structure of the samples. Field emission scanning electron microscopy (FESEM, JSM-7600F) and transmission electron microscopy (TEM, JEOL-2100) was utilized to analyze the morphology and structure of the samples. Elemental dispersive X-ray spectrum (EDS) was performed in TEM equipped with SUPER-X detector. The chemical state and valence band position of the samples were studied by X-ray photoelectron spectroscopy (XPS, PHI Quantum 2000). In-situ irradiated XPS were measured by ESCALAB 250Xi (Thermo Fisher, USA) with Al Kα source (1486.6 eV) in the absence and presence of 365 nm-light illumination. The UV-visible absorption spectra were measured by Shimadzu UV-2600 spectrophotometer. The electrochemical workstation (CHI660C) was used for transient photocurrent testing in a standard three-electrode system (working electrode: the as prepared samples; counter electrode: platinum electrode; reference electrode: Ag/AgCl (saturated KCl)). The room temperature electron paramagnetic resonance (EPR) spectra were evaluated using a Brook A200 EPR spectrometer. N_2-temperature programmed desorption (N_2-TPD) analysis was performed using Micromeritics AutoChem II. Photoluminescence (PL) spectra of the photocatalysts were performed at room temperature with an excitation wavelength of 325 nm and an excitation light source of Xe lamp. The quantification of H_2 products was carried out using gas chromatography (Shimadzu GC-7920, TCD detector, Ar carrier, molecular sieve 5 Å). The sample's mass evolution by TGA was analyzed by means of a STA PT-1600 equipment (Linseis, Selb, Germany).

Photoreduction of N_2

The photocatalytic N_2 reduction performance of F-TiO_2 was evaluated at atmospheric pressure and ambient temperature using a 300 W Xe lamp as light source. In the photocatalytic experiments, 20 mg of photocatalyst and 10 mL of methanol were dispersed in 90 mL of ultra-pure water and placed in a quartz reactor. The photocatalytic NRR experiments were started after initiating a 20°C recirculating

condensate and performing 30 min N_2 (purity ≥ 99.9%) flux (60 mL min^{-1}) in the dark state. After illumination, 2 mL of reaction solution was withdrawn at a certain interval (0h, 0.5h, 1h and 2h) for the determination of NH_4^+ concentration on a Shimadzu UV-2600 spectrometer using the colorimetric method (determined by absorbance at 420 nm) with the Nano reagent.

Electron transfer ratio calculations

The ratio of ammonia-producing to hydrogen-producing electron transfer per unit time can demonstrate the inhibition of HER for the catalyst. On the basis of the photocatalytic nitrogen fixation device, nitrogen gas transport is maintained. The outlet is connected to water, and the collected gas is collected using a drainage method. The collected gas is injected into a gas chromatograph equipped with a thermal conductivity detector (TCD) to measure the hydrogen production rate for one hour. Additionally, a dispersed solution is taken out for nanoparticle reagent method analysis of ammonia concentration. Formula for calculating the electron transfer ratio of ammonia production to hydrogen production:

$$NRR/HER = \frac{v_{NRR} * 6}{v_{HER} * 2} \times 100\%$$

Band structure calculations

Density Functional Theory (DFT) calculations were implemented in the Vienna ab initio package code by means of the Perdew-Burke-Ernzerhof (PBE) generalized gradient approximation and Projected Augmented Wave (PAW).[1,2] The Vienna Atomic Bomb Simulation Package (VASP) was utilized for all calculations. The Brillouin-zone sampling is restricted to the Gamma point in the surface geometry optimization and 1×1×1 Monkhorst-Pack in the calculation of density of states (DOS). All calculations were conducted using a plane-wave basis set with a 500 eV cutoff and the supercell, in accordance with standard computational methods. DFT calculations usually lead to a significant underestimation of the transition metal oxide band gap. In our calculations, in order to take into account the Coulomb correlation

interactions of the Ti 3d electrons, the GGA+U approach (U = 7 eV) is taken to fit to the experimental band gap.

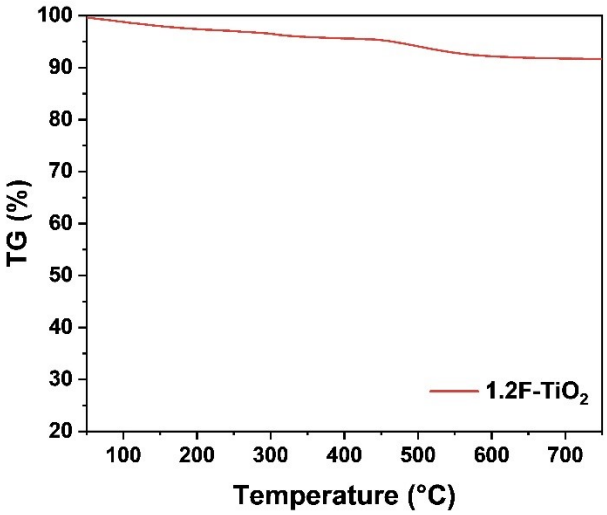

Fig. S1 TG curve of 1.2F-TiO_2.

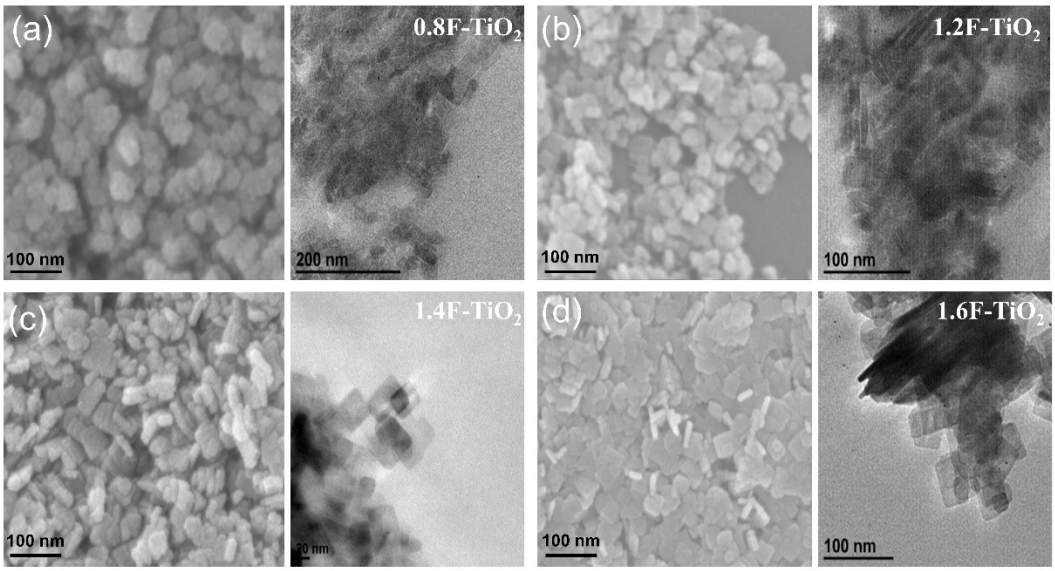

Fig. S2 TEM images of (a) 0.8F-TiO_2, (b) 1.2F-TiO_2, (c) 1.4F-TiO_2 and (d) 1.6F-TiO_2.

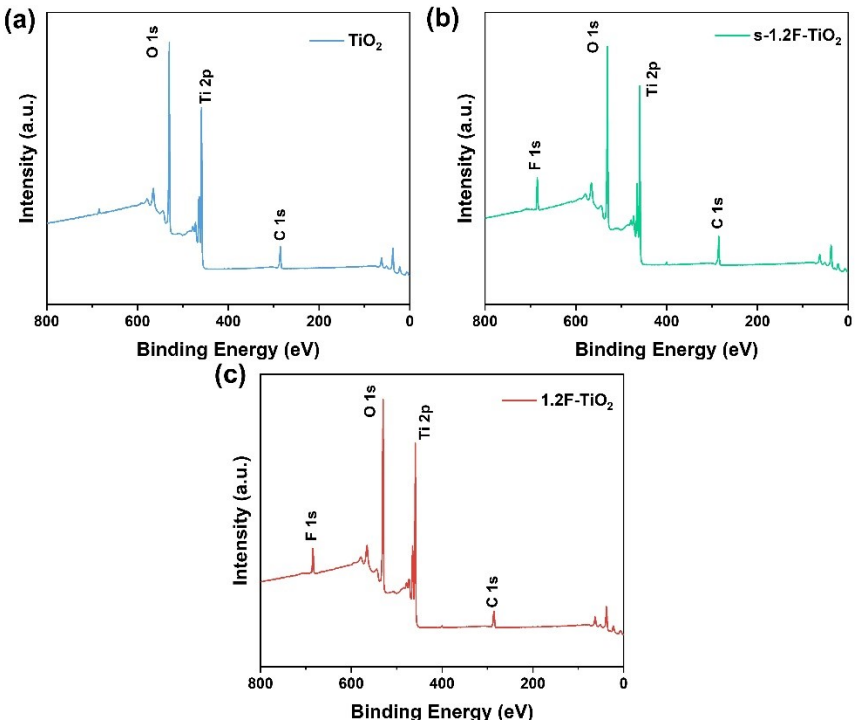

Fig. S3 Survey spectra of (a) TiO_2, (b) s-1.2F-TiO_2 and (c) 1.2F-TiO_2.

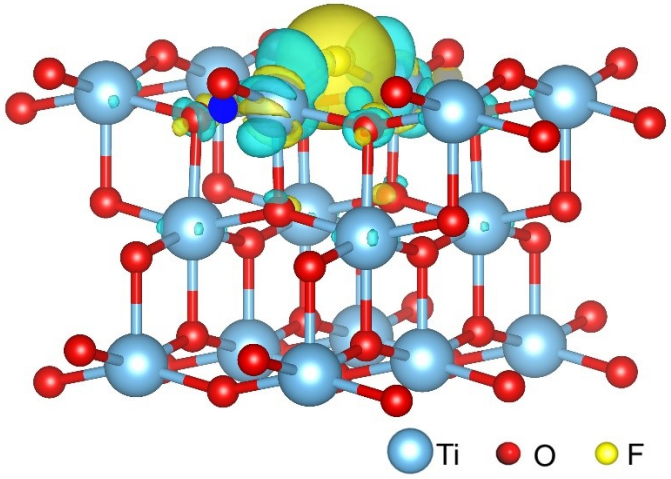

Fig. S4 The charge density difference of F-TiO_2 surface. The yellow and cyan represent electron accumulation and electron depletion, respectively.

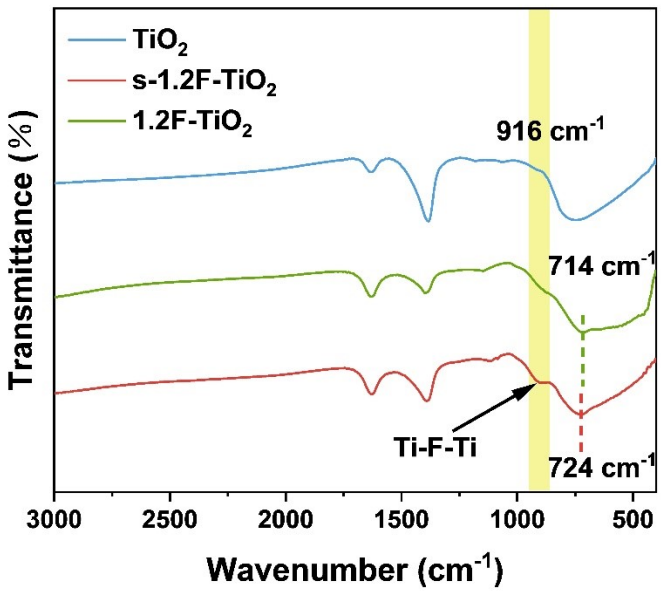

Fig. S5 FT-IR spectra of TiO_2, s-1.2F-TiO_2 and 1.2F-TiO_2.

To further verify the bonding of fluorine in the F-TiO_2 structure, the catalyst was characterized using FT-IR as shown in **Fig. S7**. The strong spectral bands around 500 cm^{-1}-800 cm^{-1} can be attributed to the telescopic vibrational modes of the Ti-O-Ti bond. Comparison of s-1.2F-TiO_2 and 1.2F-TiO_2 reveals that the Ti-O-Ti spectral bands are shifted to higher wave numbers, which may be due to the entry of surface F into the catalyst lattice after argon-hydrogen annealing. In addition, the adsorption peaks observed near 916 cm^{-1} indicate the presence of interstitial fluorine in the TiO_2 structure, suggesting the formation of Ti-F-Ti bonds. This result is consistent with the XPS analysis.

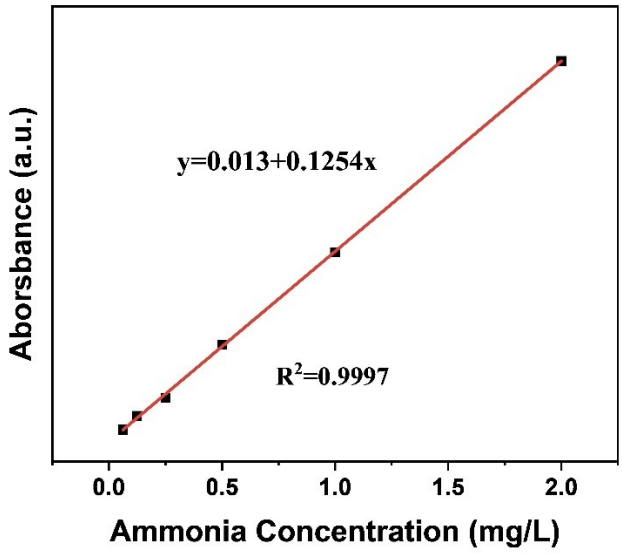

Fig. S6 Standard curves for NH_4^+ with Nessler's reagent.

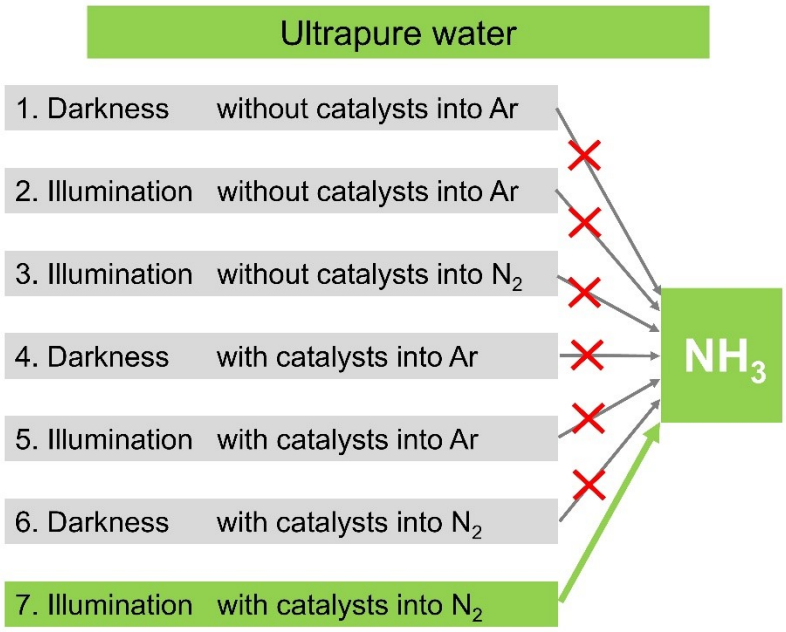

Fig. S7 Flow diagram of control experiments to confirm that NH_3 production over the investigated catalysts.

Ultrapure water was directly analyzed. In 1, 2, 4 and 5 steps, N_2 gas was passed through the testing system for 2 h, then the reaction liquid was filtered and analyzed. In 3 and 6 steps, N_2 gas was passed through the testing system for 2 h, then the reaction liquid was filtered and analyzed. In 7 step, N_2 gas was passed through the testing system for 10 h, then the reaction liquid was filtered and analyzed.

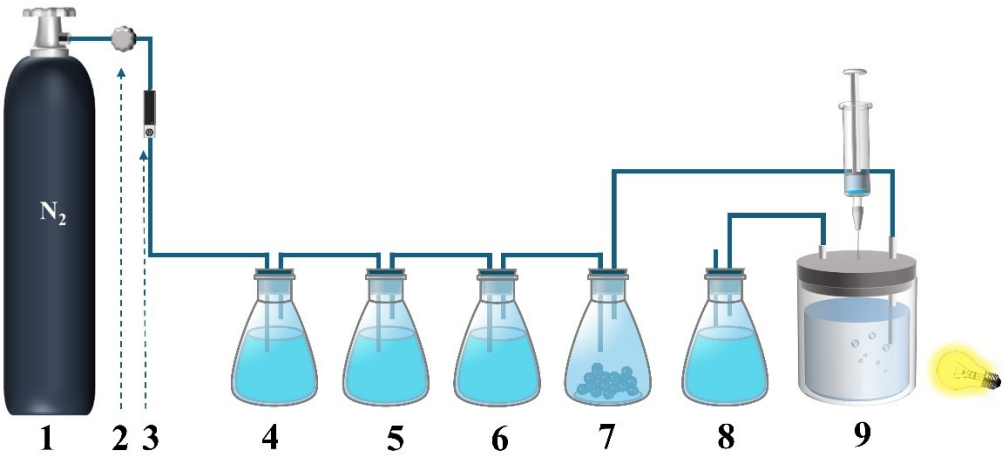

Fig. S8 Schematic illustration of NRR equipment used in the present study.

1 N_2 cylinder, 2 reducing valve, 3 mass flowmeter, 4 $FeSO_4$ (1.0 M), 5 KOH (1.0 M), 6 H_2SO_4 (1.0 M), 7 allochroic silicagel, 8 tail gas absorber, 9 reaction vessel.

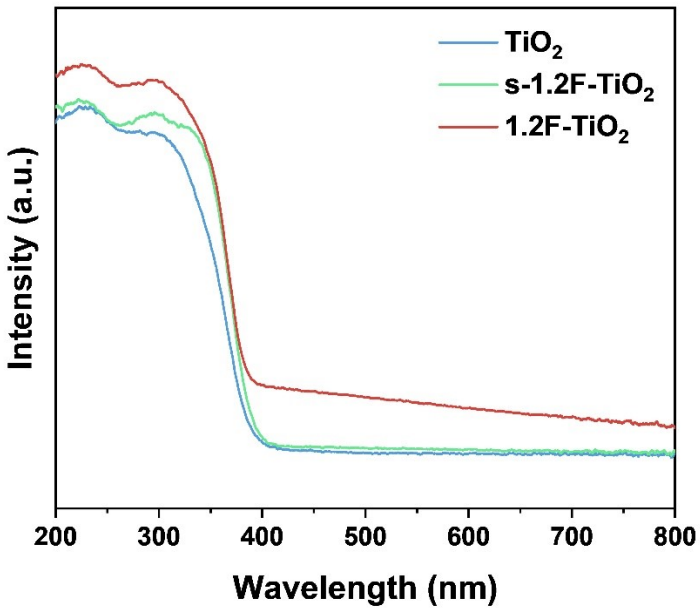

Fig. S9 UV–vis diffuse reflection spectra of TiO_2, s-1.2F-$TiO_2$and 1.2F-TiO_2.

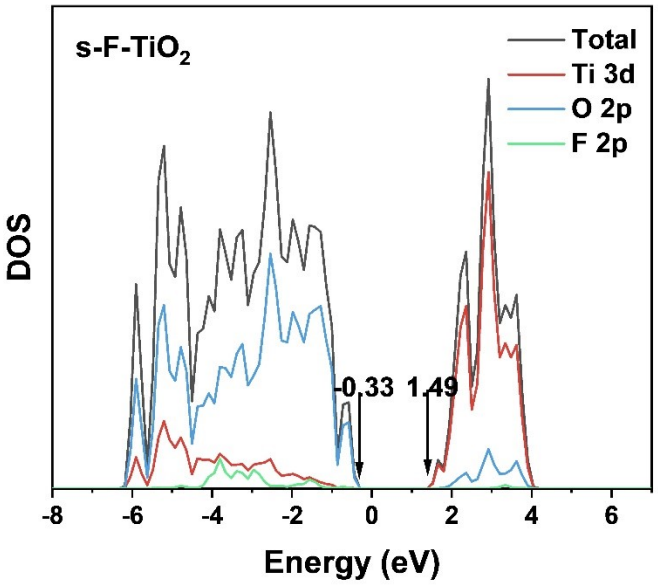

Fig. S10 The partial wave DOS of s-F-TiO_2.

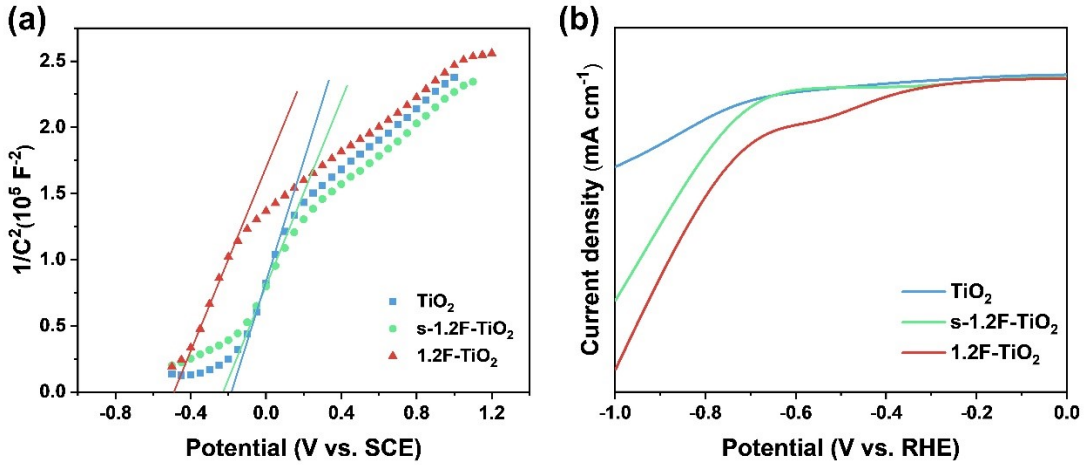

Fig. S11 TiO_2, s-1.2F-TiO_2 and 1.2F-TiO_2, (a) Mott-Schottky spectra and (b) Linear sweep voltammetry (LSV) curves.

In order to further understand the effect of fluorination on the carriers inside TiO_2, Mott-Schottky (MS) tests were performed on TiO_2, s-1.2F-TiO_2 and 1.2F-TiO_2. As shown in **Fig. S8a**, according to the MS equation, the carrier concentration of each of the three catalysts was obtained as 8.408×10^{27}, 5.970×10^{27}, 5.743×10^{27}, indicating that fluorination increased the carrier concentration. The contrasting TiO_2, s-1.2F-TiO_2, and 1.2F-TiO_2 all have similar onset potentials (**Fig. S8b**). However, at the same overpotential (0.4 V vs RHE), 1.2F-TiO_2 has a greater current density, indicating that more N_2 is reduced at the electrode.

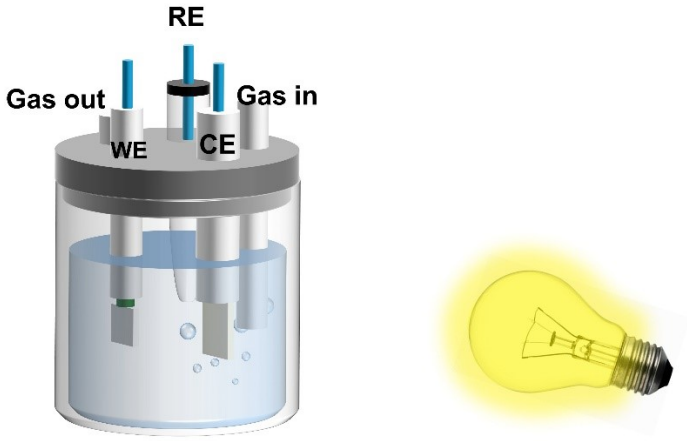

Fig. S12 Schematic illustrating the setup for the transient photocurrent measurement.

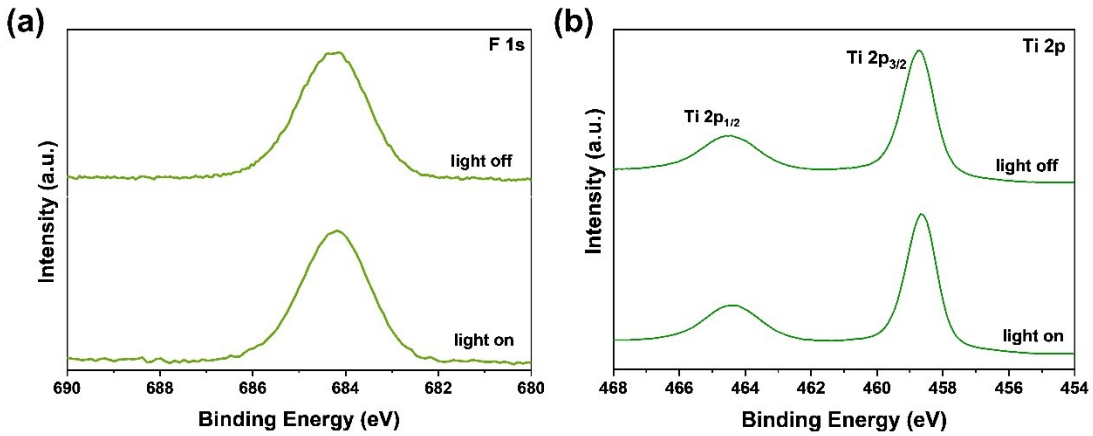

Fig. S13 High-resolution XPS spectra of (a) F 1s and (b) Ti 2p in s-1.2F-TiO_2 under 365 nm LED irradiation.

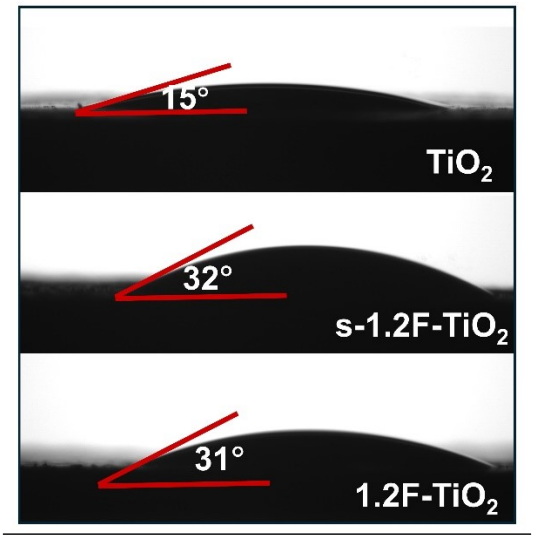

Fig. S14 Contact angle measurement of TiO_2, s-1.2F-TiO_2 and 1.2F-TiO_2 after photocatalytic nitrogen fixation.

To determine the stability of surface fluorination-induced hydrophobicity, we determined the contact angle test after the photocatalytic nitrogen fixation reaction. The resultant hydrophobicity remained essentially the same as before the reaction, indicating a good stability of the hydrophobicity after fluorination.

Tab. S1 The surface F content of (a) TiO_2 (b) s-1.2F-TiO_2 (c) 1.2F-TiO_2 according to XPS result.

(a)

Name	Start BE	Peak BE	End BE	Height CPS	FWHM eV	Area (P) CPS.eV	Area (N) TPP-2M	Atomic %
Ti2p	468.08	458.94	449.08	787074.43	2.29	3122151.93	7626.18	25.28
O1s	537.58	530.11	523.08	968398.29	2.3	2725115	15786.59	52.33
F1s	697.08	684.32	679.58	29055.99	2.6	111129.22	513.75	**0.12**
C1s	293.58	285.33	277.08	126539.89	2.83	432926.5	6072.71	22.27

(b)

Name	Start BE	Peak BE	End BE	Height CPS	FWHM eV	Area (P) CPS.eV	Area (N) TPP-2M	Atomic %
Ti2p	468.39	459.09	451.08	779746.61	2.15	3053444.32	48265.46	46.47
O1s	535.08	530.23	520.08	893930.41	2.34	2558409.08	42698.35	41.11
F1s	688.08	684.81	679.08	136771.55	1.63	397385.17	7567.95	**7.29**
C1s	291.08	285.91	277.08	99167.5	3.14	348839.25	4895.04	5.13

(c)

Name	Start BE	Peak BE	End BE	Height CPS	FWHM eV	Area (P) CPS.eV	Area (N) TPP-2M	Atomic %
Ti2p	468.58	459.21	448.58	796419.63	2.27	3139309.44	49626.97	46.66
O1s	538.08	530.39	523.08	901682.01	1.44	2707794.19	45197.25	42.49
F1s	695.58	684.99	680.58	106929.62	2.51	315040.67	6000.73	**5.64**
C1s	292.58	286.11	277.08	105443.29	3.11	360654.71	5061.49	5.21

Tab. S2 Comparing ammonia yields of photocatalysts in recent literature.

Photocatalyst	**Light source**	**NH_3 yield rate ($\mu mol\ g^{-1}h^{-1}$)**	**Reaction medium**	**Scavenger**	**Ref.**
F-TiO_2	Full spectrum (300W Xenon lamp)	**63.8**	H_2O (l)	Methanol	This work
rutile TiO_2	>420nm (300W Xenon lamp)	116	H_2O (l)	Methanol	[3]
Au/ anatase TiO_2-OV	Full spectrum (300W Xenon lamp)	76	H_2O (l)	Methanol	[4]
Ru atom decorated anatase TiO_2 nanosheets	Full spectrum (300W Xenon lamp)	3.311	H_2O (l)	Methanol	[5]
MIL-125 @rutile TiO_2 complex	Full spectrum (300W Xenon lamp)	102.7	H_2O (l)	Methanol	[6]
rutile TiO_2@C/g-C_3N_4	>420nm (300W Xenon lamp)	250.6	H_2O (l)	Methanol	[7]
AgPt−rutile TiO_2	Full spectrum (300W Xenon lamp)	38.4	H_2O (l)	No	[8]
anatase MXene/TiO_2/Co photocatalysts	Full spectrum (300W Xenon lamp)	110	H_2O (l)	No	[9]
Ni doping mesoporous anatase TiO_2	Full spectrum (300W Xenon lamp)	46.8	H_2O (l)	No	[10]
anatase Au@TiO_2 NT	Full spectrum (500W Xenon lamp)	1.09	H_2O (l)	No	[11]
anatase *p*-TiO_2 with Ti vacancies	Full spectrum (500W Xenon lamp)	64.8	H_2O (l)	No	[12]
Mo doped mesoporous anatase TiO_2	>420nm (300W Xenon lamp)	183.02	H_2O (l)	No	[13]

References

1 C. Li, T. Wang, Z. Zhao, W. Yang, J. Li, A. Li, Z. Yang, G. A. Ozin and J. Gong, *Angew. Chem. Int. Ed.*, 2018, **57**, 5278–5282.

2 Y. Jiang, W. Zhao, S. Li, S. Wang, Y. Fan, F. Wang, X. Qiu, Y. Zhu, Y. Zhang, C. Long and Z. Tang, *J. Am. Chem. Soc.*, 2022, **144**, 15977–15987.

3 Q.-Y. Liu, H.-D. Wang, R. Tang, Q. Cheng and Y.-J. Yuan, *ACS Appl. Nano Mater.*, 2021, **4**, 8674–8679.

4 J. Yang, Y. Guo, R. Jiang, F. Qin, H. Zhang, W. Lu, J. Wang and J. C. Yu, *J. Am. Chem. Soc.*, 2018, **140**, 8497–8508.

5 S. Liu, Y. Wang, S. Wang, M. You, S. Hong, T.-S. Wu, Y.-L. Soo, Z. Zhao, G. Jiang, Jieshan Qiu, B. Wang and Z. Sun, *ACS Sustain. Chem. Eng.*, 2019, **7**, 6813–6820.

6 L. Wang, S. Wang, M. Li, X. Yang, F. Li, L. Xu and Y. Zou, *J. Alloys Compd.*, 2022, **909**, 164751.

7 Q. Liu, L. Ai and J. Jiang, *J. Mater. Chem. A*, 2018, **6**, 4102–4110.

8 X. Bian, Y. Zhao, S. Zhang, D. Li, R. Shi, C. Zhou, L.-Z. Wu and T. Zhang, *ACS Mater. Lett.*, 2021, **3**, 1521–1527.

9 W. Gao, X. Li, S. Luo, Z. Luo, X. Zhang, R. Huang and M. Luo, *J. Colloid Interface Sci.*, 2021, **585**, 20–29.

10 J. Li, D. Wang, R. Guan, Y. Zhang, Z. Zhao, H. Zhai and Z. Sun, *ACS Sustain. Chem. Eng.*, 2020, **8**, 18258–18265.

11 S. Chang and X. Xu, *Inorg. Chem. Front.*, 2020, **7**, 620–624.

12 W. Ding, X. Li, S. Su, Z. Liu, Y. Cao, L. Meng, S. Yuan, W. Wei and M. Luo, *Nanoscale*, 2023, **15**, 4014–4021.

13 X. Li, J. Li, H. Zhai, M. Song, L. Wang, R. Guan, Q. Zhang and Z. Zhao, *Catal. Lett.*, 2022, **152**, 116–123.